

Observation of Raman self-focusing in an alkali-metal vapor cell

N. A. Proite, B. E. Unks, J. T. Green, and D. D. Yavuz

Department of Physics, 1150 University Avenue, University of Wisconsin at Madison, Madison, Wisconsin 53706, USA

(Received 10 October 2007; published 20 February 2008)

We report an experimental demonstration of Raman self-focusing and self-defocusing in a far-off resonant alkali-metal atomic system. The key idea is to drive a hyperfine transition in an alkali-metal atom to a maximally coherent state with two laser beams. In this regime, the two-photon detuning from the Raman resonance controls the nonlinear index of the medium.

DOI: 10.1103/PhysRevA.77.023819

PACS number(s): 42.50.Gy, 42.65.Dr, 42.65.Jx, 42.65.Tg

Over the last decade there has been a growing interest in effects that utilize atomic coherence to manipulate the propagation of light inside a medium [1]. As an example, using an appropriately phased Raman coherence, one can render a medium transparent to a resonant laser beam with the technique of electromagnetically induced transparency (EIT) [2–4]. For nonlinear mixing processes, the concept of maximum atomic coherence is particularly important. It is now understood that frequency conversion in the regime of maximum coherence proceeds very efficiently with phase-matching playing a negligible role [5–7]. In resonant, EIT-like systems, a maximally coherent state is adiabatically prepared using a counterintuitive pulse timing sequence. In far-off resonant atomic systems, which is the case in this work, preparation is achieved with two laser beams whose frequency difference is slightly detuned from the frequency of the two-photon Raman transition.

When a dipole-forbidden Raman transition is driven to a maximally coherent state, the population is almost equally split between the two Raman states, and the off-diagonal density matrix element of the transition approaches its maximum value, $\rho \approx 1/2$. In far-off resonant systems, one important consequence of maximum coherence is the modification of the refractive indices of the driving laser beams [8,9]. Noting Fig. 1, depending on the sign of the two-photon detuning, $\Delta\omega$, the established atomic coherence is either in-phase or π out-of-phase with the strong two-photon drive. As a result, the refractive indices of the two driving lasers, E_p and E_s , are either enhanced ($\Delta\omega > 0$) or reduced ($\Delta\omega < 0$). The modification of the refractive indices is intensity dependent and varies across the spatial profile of the beams. As a result, the medium acts as a lens causing self-focusing or self-defocusing of the driving lasers. One important application of Raman self-focusing is to the field of spatial optical solitons. It has recently been predicted that, under appropriate conditions, diffraction may be balanced by Raman self-focusing and as a result two-frequency optical solitons are formed [10–12]. In alkali-metal vapor cells, the formation of these solitons, termed spatial Raman solitons, require low optical power (≈ 100 mW) that is readily achievable with continuous-wave (cw) lasers. Due to operating near maximum coherence, $\rho \approx 1/2$, these solitons are stable in full three spatial dimensions. Numerical simulations of these solitons predict well-defined soliton-soliton collision properties and reveal many rich nonlinear dynamics [12]. Spatial Raman solitons in alkali-metal vapor cells may also find pos-

sible practical applications in areas such as all-optical information processing [13,14].

In this paper, we utilize the hyperfine transition between $F=1$ and $F=2$ levels and demonstrate Raman self-focusing and self-defocusing of the two driving laser beams, E_p and E_s , in a ^{87}Rb vapor cell. Before proceeding with a detailed description of our experiment, we would like to cite pertinent earlier work. By using high-peak power, Q -switched pulsed lasers, Harris group at Stanford has recently demonstrated Raman self-focusing in molecular hydrogen (H_2) [15]. Self-focusing in a resonant, three level Λ scheme under the conditions of EIT was observed by Moseley and colleagues [16,17]. Optical wave-guiding in a V scheme by using strong optical pumping was demonstrated by Truscott *et al.* [18]. There has been substantial theoretical work on electromagnetically induced focusing in a variety of near-resonance, multifrequency systems [18–22]. Raman gain and slow light propagation in far-off resonant ^{85}Rb alkali-metal atoms were recently demonstrated by Deng and colleagues [23]. We also

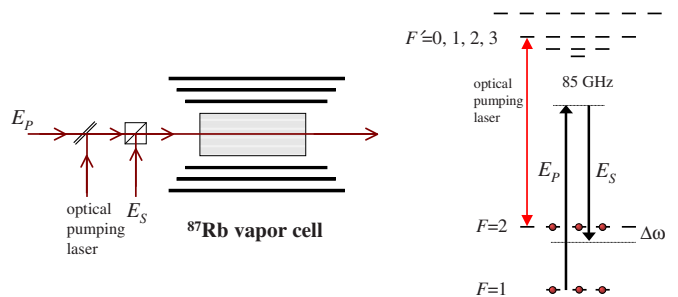


FIG. 1. (Color online) Simplified schematic of our experiment and the energy level diagram (not to scale) for ^{87}Rb . The experiment is performed in a temperature controlled triple layer magnetically shielded quartz vapor cell at an atomic density of $N \approx 1.66 \times 10^{13}$ atoms/cm 3 . An optical pumping laser tuned to the $F=2 \rightarrow F'=2$ transition of the $D2$ line optically pumps the atoms to the $F=1$ manifold. The two intense laser beams, E_p and E_s , drive the atoms to a near maximally coherent state. The two driving laser beams have orthogonal polarizations and they are detuned by 85 GHz from the $D2$ line (see text for details). The experiment works in three parallel channels with three Raman coherences prepared between the same m -states of the $F=1$ and $F=2$ levels (the quantization axis is chosen parallel to the beam propagation direction). Depending on the sign of the detuning from the Raman transition, $\Delta\omega$, the beams either self-focus or self-defocus. To observe the effect, we measure the size of the beams after they exit the cell.

note that, since the pioneering work of Ashkin and colleagues [24], a large number of experiments have demonstrated self-trapping and pattern formation of laser beams in atomic vapor cells utilizing inherently dissipative one-photon resonances [25–27].

Figure 1 shows the relevant energy level diagram and the experimental setup. We work with a triple layer magnetically shielded and temperature controlled ^{87}Rb vapor cell. Temperature control is necessary to avoid density fluctuations of the vapor. Magnetic shielding is necessary to avoid broadening and shift of the Raman transitions due to external magnetic fields. The vapor cell is $L=7.5$ cm long and contains isotopically pure ^{87}Rb and 10 torr of nitrogen (N_2) as a buffer gas. The temperature of the vapor cell is kept at $T=120$ °C. Using the vapor pressure model of Ref. [28], we calculate the atomic density to be roughly $N \approx 1.66 \times 10^{13}$ atoms/cm³. We use $F=1$ and 2 hyperfine levels of ^{87}Rb in the ground electronic state $5S_{1/2}$ as our Raman states. The Raman transition frequency is the hyperfine splitting which is 6.834 GHz and the two photon detuning from the Raman resonance is defined as $\Delta\omega = 2\pi \times 6.834 \text{ GHz} - (\omega_p - \omega_s)$. For Raman transition between these two levels we utilize far-off resonant excitation through the excited electronic state $5P_{3/2}$ ($D2$ line) near a wavelength of $\lambda = 780.2$ nm.

The experiment starts with optical pumping of the ^{87}Rb atoms to the $F=1$ ground state manifold. This is achieved with an optical pumping laser that is saturation absorption locked to a $F=2 \rightarrow F'=2$ transition of the $D2$ line. To obtain the necessary amount of power, we use an external cavity diode laser amplified by a semiconductor tapered amplifier. The use of N_2 as a buffer gas greatly alleviates problems due to radiation trapping during the optical pumping process. We find that, with an optical power of about 300 mW in a beam size of $W_0=0.57$ mm, we can optically pump a large fraction of the atoms to the $F=1$ ground state manifold. Once the optical pumping beam is switched off, the atoms relax back to the $F=2$ level due to spin exchange collisions. We measure this relaxation time to be about 50 μs , which is also the time window to perform the experiment.

Once the optical pumping laser is switched off, we turn on the two driving laser beams (termed the pump beam, E_p , and the Stokes beam, E_s). The optical power in each beam is 250 mW and the beams have a collimated beam waist of $W_0=0.57$ mm at the vapor cell. Since we are working in a hot vapor cell, collinear propagation of the two beams is critical in order to avoid two-photon Doppler broadening. We guarantee perfect overlap by coupling all the laser beams into a single mode, polarization maintaining fiber before the vapor cell (not shown in Fig. 1). The two laser beams have orthogonal linear polarizations at the vapor cell with a polarization purity at the 1% level.

The two driving laser beams, E_p and E_s , are obtained from the same external cavity diode laser. To obtain the required frequency shift of 6.834 GHz, we use two high-frequency acousto-optic modulators in a double pass configuration. Each frequency-shifted beam is then amplified with semiconductor tapered amplifiers to obtain required power levels. This setup produces about an order of magnitude more opti-

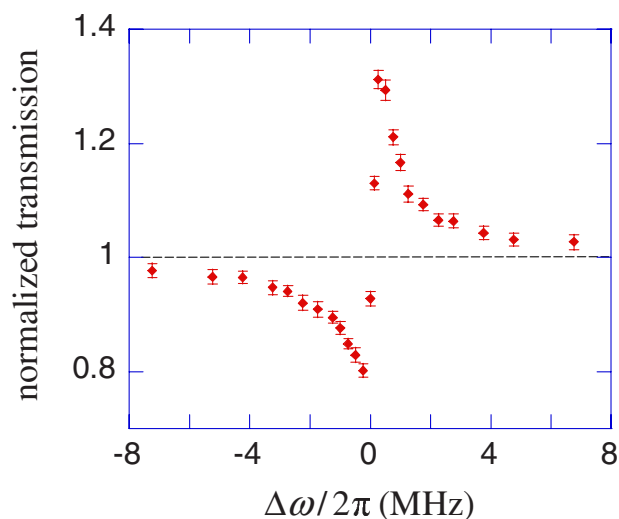


FIG. 2. (Color online) Transmission of the two laser beams through a 150 μm pinhole as a function of the two-photon detuning, $\Delta\omega$. The dashed line is the transmission in the absence of the Raman interaction (freely propagating beam). The beam width reaches its maximum and minimum values off-resonance demonstrating the Raman self-focusing and defocusing effect. We see an abrupt transition from beam maximum to minimum while scanning through the Raman resonance. For large values of the detuning $\Delta\omega$, the atomic coherence decreases and the beam width approaches the value of a freely propagating beam (dashed line).

cal power (250 mW for each beam at the vapor cell) when compared with previous approaches for addressing hyperfine transitions in alkali-metal atoms. Furthermore, the relative frequency stability between the two laser beams is at the 1 Hz level. Further details regarding our laser system can be found in our recent publication [29]. The one-photon detuning of the two lasers from the excited electronic state $5P_{3/2}$ is 85 GHz, which is large when compared with the Doppler linewidth of this state (650 MHz). The system is, therefore, a far-off resonant system and the Raman interaction is the dominant interaction of the two lasers with the atomic vapor.

The optical pumping process does not pump to a specific m state in the ground $F=1$ manifold. As a result, after the optical pumping process, the atoms are distributed to all three m states at the $F=1$ level. The experiment, therefore, works in three parallel channels and three Raman coherences: $\rho_{-1,-1}$ ($|F=1, m_F=-1\rangle \rightarrow |F=2, m_F=-1\rangle$), $\rho_{0,0}$ ($|F=1, m_F=0\rangle \rightarrow |F=2, m_F=0\rangle$), and $\rho_{1,1}$ ($|F=1, m_F=1\rangle \rightarrow |F=2, m_F=1\rangle$), are driven with the two laser beams. To allow adiabatic preparation of the Raman coherences, we turn on the two lasers smoothly over about 4 μs . In this regime, depending on the sign of the Raman detuning, $\Delta\omega$, the established Raman coherences are either in phase ($\Delta\omega > 0$) or π out of phase ($\Delta\omega < 0$) with the two-photon driving force [8,9]. As a result, the refractive indices of the driving lasers are either enhanced or reduced. For the parameters of our experiment, the medium acts like a thin lens producing a curved phase front on the beams at the end of the vapor cell. There is not a significant change in the spatial profile of the beams inside the medium. After the beams exit the vapor cell, their beam size is measured 75 cm away from the cell

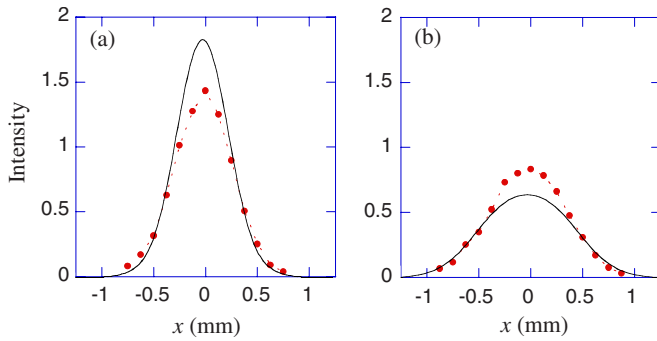


FIG. 3. (Color online) The data points are the spatial profiles of the two driving laser beams (a) for the focused ($\Delta\omega=2\pi \times 0.25$ MHz) and (b) for the defocused ($\Delta\omega=2\pi \times -0.25$ MHz) cases. The measured FWHM size of the beams is 0.64 mm (a) and 0.88 mm (b), respectively. The solid curve in each plot is the result of a numerical simulation for each experiment without any adjustable parameters. The agreement between the experimental results and the numerical simulations is reasonably good for both cases.

by monitoring the amount of transmitted power through a $150 \mu\text{m}$ pinhole.

Figure 2 shows the normalized transmitted power of the two laser beams through the pinhole. The dashed line is the transmission in the absence of the Raman interaction (freely propagating beam). The transmission, and therefore the size of the beams, reaches its maximum and minimum values off resonance demonstrating the Raman self-focusing and defocusing effect. We see an abrupt transition from beam maximum to beam minimum while scanning through the Raman resonance. For large values of the detuning $\Delta\omega$, the atomic coherence decreases and the beam width approaches the value of a freely propagating beam (dashed line). The beam size reaches its maximum and minimum values at $\Delta\omega=2\pi \times -0.25$ MHz, and $\Delta\omega=2\pi \times 0.25$ MHz, respectively. We calculate the value of the coherence of the Raman transitions at the intensity peak of the lasers to be $\rho=-0.46$ (for $\Delta\omega=2\pi \times -0.25$ MHz) and $\rho=0.49$ (for $\Delta\omega=2\pi \times 0.25$ MHz), respectively (for all three channels). The established atomic coherence is slightly larger for the positive detuning due to the Stark shift of the Raman resonance. For $\Delta\omega>0$, the Stark shift tunes the driving lasers closer to Raman resonance as the laser intensities are increased. This is also the reason for the slight asymmetry between the two sides of the resonance in the transmission data of Fig. 2.

Figure 3 shows the experimentally measured spatial profiles of the two driving laser beams for the focused ($\Delta\omega=2\pi \times 0.25$ MHz) and defocused ($\Delta\omega=2\pi \times -0.25$ MHz) cases. These profiles are recorded 75 cm away from the cell by moving the pinhole with a translation stage. Similar to Fig. 2, the intensities are normalized such that one unit in the plots corresponds to the peak intensity of a freely propagating beam (in the absence of Raman interaction). When the beams are focused and defocused their measured full width at half maximum (FWHM) sizes are 0.64 and 0.88 mm, respectively. The solid curves in each plot are the results of numerical calculations for our experiment without any fitting parameters. The assumptions that we make in these numerical calculations are (1) we neglect the residual two-photon

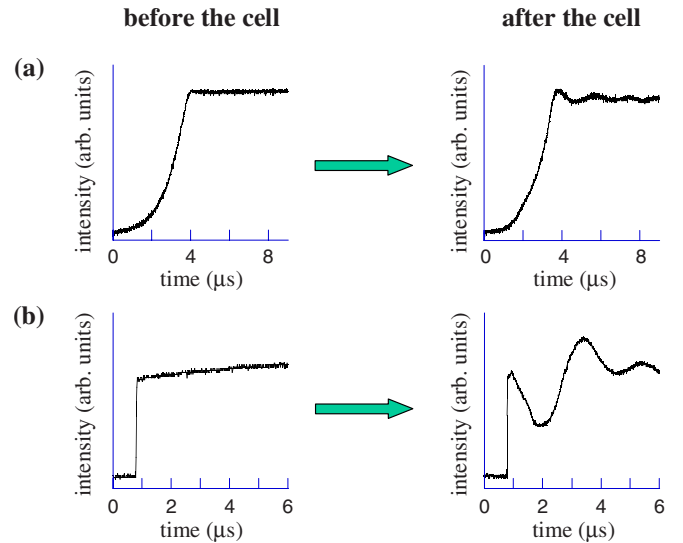


FIG. 4. (Color online) The temporal profiles for the pump laser beam, E_p , measured before and after the vapor cell. In (a), the pump laser smoothly turns on to its peak value in about $4 \mu\text{s}$. Here, the atomic evolution is adiabatic and the pump laser largely preserves its smooth nature as it propagates through the vapor cell. In (b), we turn on the pump laser sharply. As a result, the evolution is non-adiabatic, and the atomic population undergoes two-photon Rabi oscillations between the two levels. This oscillation results in large variations in the amplitude of the pump laser as it leaves the vapor cell. To allow adiabatic preparation of an appropriately phased Raman coherence, all the measurements of Figs. 2 and 3 were performed with the smooth profiles of (a).

Doppler broadening due to the finite size of the beams; (2) we ignore atomic motion since the diffusion of atoms during the time scales of interest is much smaller when compared with the size of the beams; and (3) we ignore relaxation processes since our pulse widths are much shorter when compared with the relevant relaxation times. With these assumptions, we solve the slowly varying envelope propagation equations for the two laser beams in full three spatial dimensions (two transverse dimensions and one propagation dimension) simultaneously with the adiabatic solution for the atomic system. The propagation of the two laser beams is coupled to each other through the established hyperfine coherences in three parallel channels. Further details with regard to the numerical simulations can be found in Ref. [12]. The agreement between our numerical calculations and the experimental results is reasonably good for both cases.

We next discuss the adiabatic preparation of the medium. As shown in Fig. 4(a), to adiabatically prepare a maximally coherent state, we turn on the two driving laser pulses smoothly in about $4 \mu\text{s}$. We then make our measurements at the peak of the pulses. Figure 4 contrasts adiabatic and non-adiabatic evolution of the atomic system. Here we plot the total power (measured without the pinhole) of the pump beam E_p before and after the vapor cell for a two-photon detuning of $\Delta\omega=2\pi \times 0.25$ MHz. In part (a), the evolution is adiabatic, and the temporal profile of the pump beam largely retains its smooth nature after propagating through the vapor cell. In part (b), we turn on the laser beams sharply, and as a result, the atomic population undergoes two-photon

Rabi oscillations between the two hyperfine levels. This oscillation is reflected in periodic absorption and amplification of the pump beam measured after the cell. Due to the Gaussian intensity distribution in the vapor cell, atoms at different positions along the spatial profile of the laser beams undergo Rabi oscillations at different rates. As a result, the Rabi-oscillation time dynamics are complicated and cannot be explained with a single two-photon Rabi frequency [30]. All the measurements of Figs. 2 and 3 were performed with the smooth profiles of Fig. 4(a).

In conclusion, we have observed Raman self-focusing and self-defocusing in a vapor cell of ^{87}Rb alkali-metal atoms. The key idea is to adiabatically prepare the hyperfine transitions in a maximally coherent state. Our approach achieves very large nonlinearities in a far-off resonant system and does not suffer from dissipation due to excited state spontaneous emission. If we ignore the saturation of the nonlinearity due to operating near maximum coherence, the Raman

self-focusing effect can be modeled as an intensity dependent refractive index. For $\Delta\omega=2\pi\times 0.25$ MHz, the value of the nonlinear index achieved in our experiment is $n_2=1.6\times 10^{-7}$ cm²/W. The parameters of our experiment are similar to the numerical simulations where formation and collisions of spatial Raman solitons are predicted [12]. To observe these solitons, we plan to focus our beams to spot sizes of about $W_0=100$ μm and demonstrate diffraction free propagation for distances much larger than the Rayleigh length of the beam.

We thank Thad Walker for suggesting the use of N_2 as a buffer gas to eliminate the issues due to radiation trapping during the optical pumping process. We also thank Dan Sikes, Angie Parker, and Chris Deviley for assistance with the experiment. This work was supported by start-up funds from the University of Wisconsin at Madison.

-
- [1] M. O. Scully and M. S. Zubairy, *Quantum Optics* (Cambridge University Press, Cambridge, England, 1997).
- [2] S. E. Harris, *Phys. Today* **50**(7), 36 (1997).
- [3] M. D. Lukin, *Rev. Mod. Phys.* **75**, 457 (2003).
- [4] M. Fleischhauer, A. Imamoglu, and J. P. Marangos, *Rev. Mod. Phys.* **77**, 633 (2005).
- [5] M. Jain, H. Xia, G. Y. Yin, A. J. Merriam, and S. E. Harris, *Phys. Rev. Lett.* **77**, 4326 (1996).
- [6] A. J. Merriam, S. J. Sharpe, H. Xia, D. Manuszak, G. Y. Yin, and S. E. Harris, *Opt. Lett.* **24**, 625 (1999).
- [7] A. V. Sokolov, D. R. Walker, D. D. Yavuz, G. Y. Yin, and S. E. Harris, *Phys. Rev. Lett.* **85**, 562 (2000).
- [8] S. E. Harris and A. V. Sokolov, *Phys. Rev. A* **55**, R4019 (1997).
- [9] S. E. Harris and A. V. Sokolov, *Phys. Rev. Lett.* **81**, 2894 (1998).
- [10] D. D. Yavuz, D. R. Walker, and M. Y. Shverdin, *Phys. Rev. A* **67**, 041803(R) (2003).
- [11] M. Y. Shverdin, D. D. Yavuz, and D. R. Walker, *Phys. Rev. A* **69**, 031801(R) (2004).
- [12] D. D. Yavuz, *Phys. Rev. A* **75**, 041802(R) (2007).
- [13] G. I. Stegeman and M. Segev, *Science* **286**, 1518 (1999).
- [14] S. Trillo and W. Torruellas, *Spatial Solitons* (Springer-Verlag, Berlin, 2001).
- [15] D. R. Walker, D. D. Yavuz, M. Y. Shverdin, G. Y. Yin, A. V. Sokolov, and S. E. Harris, *Opt. Lett.* **27**, 2094 (2002).
- [16] R. R. Moseley, S. Shepherd, D. J. Fulton, B. D. Sinclair, and M. H. Dunn, *Phys. Rev. Lett.* **74**, 670 (1995).
- [17] R. R. Moseley, S. Shepherd, D. J. Fulton, B. D. Sinclair, and M. H. Dunn, *Phys. Rev. A* **53**, 408 (1996).
- [18] A. G. Truscott, M. E. J. Friese, N. R. Heckenberg, and H. Rubinsztein-Dunlop, *Phys. Rev. Lett.* **82**, 1438 (1999).
- [19] J. T. Manassah and B. Gross, *Opt. Commun.* **124**, 418 (1996).
- [20] R. Kapoor and G. S. Agarwal, *Phys. Rev. A* **61**, 053818 (2000).
- [21] T. Hong, *Phys. Rev. Lett.* **90**, 183901 (2003).
- [22] H. Shpaysman, A. D. Wilson-Gordon, and H. Friedmann, *Phys. Rev. A* **71**, 043812 (2005).
- [23] K. J. Jiang, L. Deng, and M. G. Payne, *Phys. Rev. A* **74**, 041803(R) (2006).
- [24] J. E. Bjorkholm and A. Ashkin, *Phys. Rev. Lett.* **32**, 129 (1974).
- [25] G. Grynberg, A. Maître, and A. Petrossian, *Phys. Rev. Lett.* **72**, 2379 (1994).
- [26] R. S. Bennink, V. Wong, A. M. Marino, D. L. Aronstein, R. W. Boyd, C. R. Stroud, S. Lukishova, and D. J. Gauthier, *Phys. Rev. Lett.* **88**, 113901 (2002).
- [27] B. Schapers, T. Ackemann, and W. Lange, *IEEE J. Quantum Electron.* **39**, 227 (2003).
- [28] D. A. Steck, Los Alamos National Laboratory Technical Report, 2001 (unpublished).
- [29] B. E. Unks, N. A. Proite, and D. D. Yavuz, *Rev. Sci. Instrum.* **78**, 083108 (2007).
- [30] We do observe the general characteristics of a Rabi-oscillation behavior. As an example, as we detune further from the two-photon Raman resonance, Rabi oscillation frequency increases and oscillation amplitude decreases.